A Wavetrap-Based Decoupling Technique for 45°-Polarized MIMO Antenna Arrays

Zhang, Yiming; Zhang, Shuai; Li, Jia-Lin; Pedersen, Gert Frølund

Published in:
IEEE Transactions on Antennas and Propagation

DOI (link to publication from Publisher):
10.1109/TAP.2019.2948531

Publication date:
2020

Document Version
Accepted author manuscript, peer reviewed version

Citation for published version (APA):
Zhang, Y., Zhang, S., Li, J.-L., & Pedersen, G. F. (2020). A Wavetrap-Based Decoupling Technique for 45°-Polarized MIMO Antenna Arrays. *IEEE Transactions on Antennas and Propagation*, *68*(3), 2148-2157. Article 8883214. https://doi.org/10.1109/TAP.2019.2948531

A Wavetrap-Based Decoupling Technique for 45°-Polarized MIMO Antenna Arrays

Yi-Ming Zhang, *Member, IEEE*, Shuai Zhang, *Senior Member, IEEE*, Jia-Lin Li, and Gert Frølund Pedersen, *Senior Member, IEEE*

***Abstract*—A decoupling method using wavetrap technique for large-scale multiple-input multiple-output (MIMO) antenna arrays consisting of 45°-polarized patch antennas is presented and studied in this paper. To achieve high isolation responses among the array elements, simple wavetrap structures are proposed and positioned around every single patch element. With the presented decoupling scheme, the strong mutual coupling between both adjacent and non-adjacent patch elements are suppressed to a low level. Theoretical and numerical studies are carried out to verify the decoupling performance of the proposed architecture. For demonstration purposes, two practical examples of 1×8 and 4×2 45°-polarized arrays centered at 4.9 GHz are developed, fabricated and measured. Results indicate that all mutual couplings among the arrays are significantly suppressed to almost less than –25 dB from 4.8 to 5.0 GHz, with a small insertion loss of around 0.7 dB, making the proposed decoupling scheme attractive and valuable for phased array and massive MIMO systems.**

***Index Terms*—Multiple-input and multiple-output (MIMO), phased array, wavetrap, massive MIMO, wideband decoupling.**

I. Introduction

MASSIVE multiple-input multiple-output (MIMO) technology is considered as a key architecture for future wireless communications to improve data throughput and energy efficiency [1], [2]. In massive MIMO systems, antenna arrays with a larger number of elements are essential as the base station antennas for serving multi-users. A small center distance between adjacent antenna elements, generally half of the free space wavelength, is required for realizing wide-angle scanning with no visible grating lobes [3]. On this occasion, strong mutual coupling between both adjacent and nonadjacent antenna elements might be generated. For a MIMO antenna array, the isolation of 17 dB between antenna elements would satisfy the requirements of error rate and MIMO capacity, as reviewed in [4]. However, such an isolation level cannot maintain the stability of massive MIMO arrays (or large-scale phased arrays) in practice [5]-[9]. The worst active VSWR, for instance, would be higher than six if the mutual coupling is around −15 dB and still over two with the coupling of −20 dB [5], [6], leading to the degradation on the maximum scanning angle or scanning accuracy. If the mutual coupling can be suppressed to less than −25 dB, the active impedance matching performance would be highly improved and the influence of the mutual coupling can be negligible. Moreover, recently, it is very popular to place a power amplifier (PA) between a phase shifter and an antenna in each RF chain of a massive MIMO transmitter. In this architecture, the loss introduced by phase shifters is much smaller, but the mutual coupling among antenna elements may result in severe distortion of PA performance. In industry, the isolation between antennas is preferred to be over 25 dB to minimize this distortion in a massive MIMO array. Therefore, a caution is given that the strong mutual coupling among antenna elements should be suppressed to a very small level, i.e., less than −25 dB or even lower.

To date, many efforts have been devoted to suppressing the mutual coupling between the antenna elements in MIMO arrays. Using electromagnetic-bandgap structures [10], [11] or resonators [12] is a common method to suppress the surface current between antennas, leading to improved isolation at the cost of bulky systems. On the other hand, *LC*-based [13]-[15] and transmission-line-based [16], [17] decoupling networks have been widely studied since the decoupling networks are independent of the antenna types, with the drawbacks of high insertion losses and/or narrow decoupling bandwidths. Recently, self-decoupled methods for two-element arrays were reported in [18] and [19]. By employing the additional structures directly connected to the antennas, the coupling among the two-element arrays can be suppressed. However, the aforementioned decoupling networks and self-decoupled methods mainly focused on two-element arrays, and did not provide effective approaches for massive MIMO arrays.

More recently, some decoupling schemes have been presented for large-scale antenna arrays [6], [20], [21]. In [6], an architecture called antenna decoupling surface was proposed and studied for massive MIMO arrays, where the isolation between adjacent antenna elements can be enhanced to higher than 25 dB at the center frequency of 2.45 GHz. Since the additional decoupling surface was normally positioned quarter-wavelength away from the antenna array, the array system was bulky. A near-field decoupling resonator was

This work was supported by AAU Young Talent Program. (*Corresponding author*: *Shuai Zhang*.)

Yi-Ming Zhang and Jia-Lin Li are with the School of Physics, University of Electronic Science and Technology of China, Chengdu 610054, China. Yi-Ming Zhang is also with the Antenna, Propagation and Millimeter-wave Systems (APMS) Section, Aalborg University, Aalborg 9220, Denmark (e-mail: yiming@es.aau.dk, jialinli@uestc.edu.cn).

Shuai Zhang and Gert Frølund Pedersen are with the Antenna, Propagation and Millimeter-wave Systems (APMS) Section, Aalborg University, Aalborg 9220, Denmark (e-mail: sz@es.aau.dk, gfp@es.aau.dk).

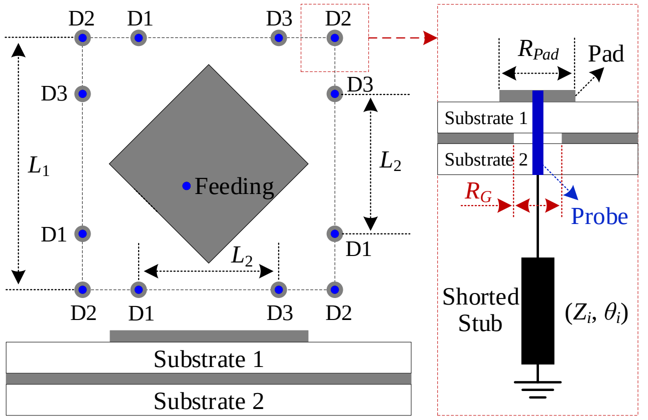

Fig. 1. Configuration of a 45°-polarized patch antenna integrated with the proposed decoupling wavetraps.

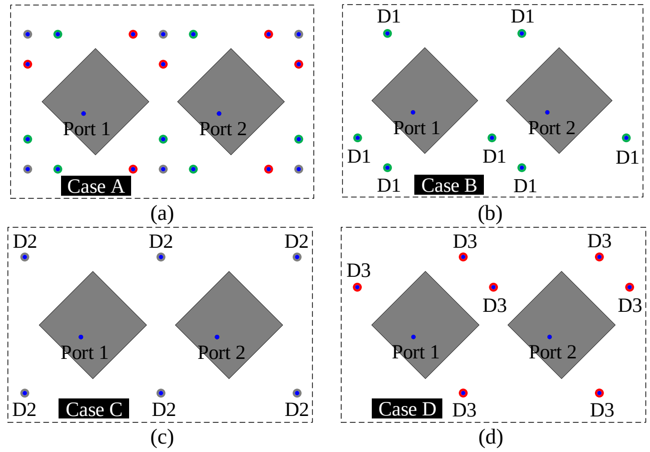

Fig. 2. Configurations of the 1×2 antenna array integrated with the proposed decoupling technique. (a) Case A. (b) Case B. (c) Case C. (d) Case D.

presented for linear antenna arrays in [20]. The isolation between adjacent antenna elements in a 1×8 patch antenna array was improved from 12 dB to 22 dB. Due to the near-field coupling effect, the resonance of the antenna elements was departed from 2.37 GHz to 2.24 GHz, with the operation band ($S_{11} \leq -10$ dB) of 2.237-2.246 GHz after decoupling. In [21], a transmission-line-based decoupling network was studied for dual-polarized large-scale arrays, where the realized isolation bandwidth featured a narrow response.

In this paper, a wavetrap-based decoupling method is proposed for 45°-polarized large-scale patch antenna arrays. Three groups of wavetraps are loaded around each patch element, leading to high-isolation responses within the antenna arrays consisting of the proposed wavetraps and the 45°-polarized patches. Compared with the previously reported literature, the main contributions and novelties of this paper are as follows:

(1) Multi-resonance decoupling responses are realized to improve the isolation bandwidth;

(2) The mutual couplings between adjacent and non-adjacent antenna elements are all well suppressed;

(3) The proposed decoupling method is with simple realization and low profile, and has nearly no effect on radiation patterns with small insertion losses.

This paper is organized as follows. Section II provides the network-based analysis of the proposed decoupling wavetrap structures. A numerical study of a 1×2 array with the proposed decoupling method is performed in Section III. In Section IV, two decoupled demonstrators of 1×8 and 4×2 arrays are developed and measured. The conclusion is stated in Section V.

II. Analysis of the Proposed Decoupling Technique

Fig. 1 shows a 45°-polarized patch antenna with the proposed wavetrap-based decoupling structure. Two stacked substrates are employed. The patch is printed on the top of substrate 1, and the ground plane is inserted between substrate 1 and substrate 2. Twelve wavetraps are positioned around the radiation patch along the boundary of a square, and separated into three groups (marked as groups D1, D2, and D3). Wavetraps belonged to group D2 are distributed at the four corners of the square, and the ones belonging to groups D1 and D3 are positioned under rotational symmetry. As illustrated in Fig. 1, a single wavetrap consists of a small metal pad printed on the top of substrate 1, a shorted stub placed on the bottom of substrate 2, and a probe through the two substrates as the connection between the pad and the stub. The shorted stubs allocated in the same group are with the same characteristic impedance and electrical length, which are Z_1 and θ_1, Z_2 and θ_2, Z_3 and θ_3 for groups D1, D2, and D3, correspondingly. Moreover, for compactness purposes, the wavetraps should not be positioned among a large area. On the other hand, adjacent wavetraps should be with certain distances to keep the independence of each wavetrap structure. Therefore, the side length of the square is set as $L_1 = 0.5\lambda_0$, and the distance between the ones belonging to D1 and D3 at the same side of the square is optimized to $L_2 = 0.28\lambda_0$, where λ_0 is the free-space wavelength. For the arrays composed of the proposed structure shown in Fig. 1, the mutual coupling among the antenna elements can be well suppressed by selecting the parameters of the shorted stubs.

Fig. 2(a) shows a 1×2 array composed of the proposed configuration plotted in Fig. 1. Based on the three groups of the wavetraps, the array is simplified to three different cases as shown in Figs. 2(b), 2(c), and 2(d). Each group of the wavetraps would feature a decoupling function at the desired frequency, which is determined by the parameter values of the shorted stubs. Taking case B given in Fig. 2(b) as the study case, the following discussion will explain the decoupling theory and give a network-based study for determining the values of parameters Z_i and θ_i, where i = 1, 2, 3. Since the isolation between ports 1 and 2 should be mainly determined by the wavetraps positioned in the area between the two radiation patches, a further-simplified configuration for case B is provided as described in Fig. 3(a). Three wavetraps are marked as $D1_A$, $D1_B$, and $D1_C$. Fig. 3(b) depicts the equivalent circuit of the two-port structure given in Fig. 3(a). Herein, *RLC* resonators ($R_P L_P C_P$) represent the radiation patches. In addition to the original coupling path, three decoupling paths are generated owing to the employed wavetraps. Therefore, there are totally four transmission paths between ports 1 and 2, and the simplified network model is shown in Fig. 3(c) describing

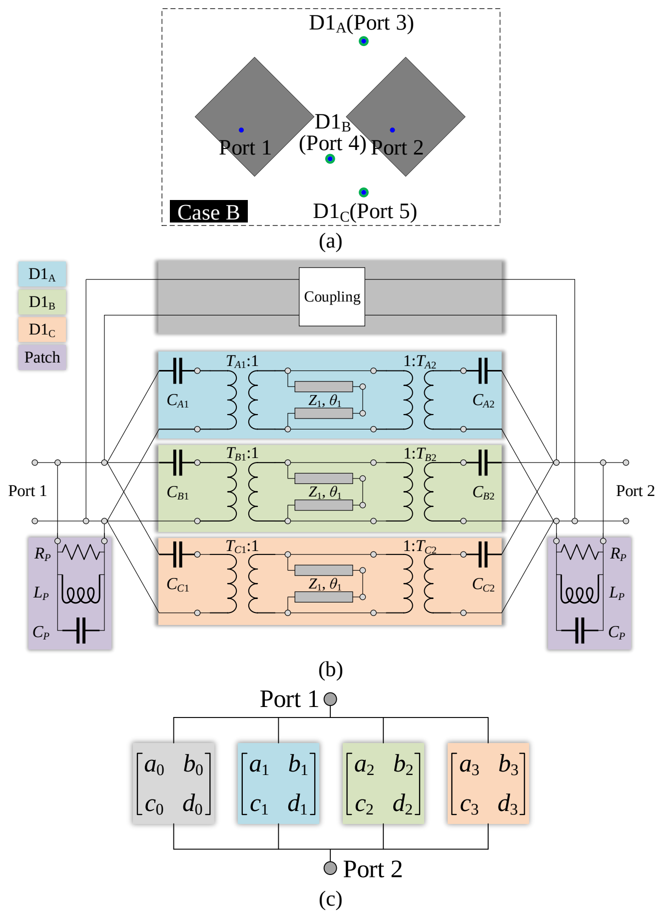

Fig. 3. (a) Simplified configuration of case B. (b) Equivalent circuit. (c) Simplified transmission model between port 1 and port 2 through the four coupling paths.

by transmission matrices. The *abcd* matrices denote the transmission responses between the patches, where the different subscripts represent the original coupling and the three additional coupling paths determined by the three wavetraps, where the *b*-parameters are formulated as

$$b_1 = \frac{-1}{\omega T_{A2} C_{A2}} \left(T_{A1} + \frac{Y_S}{\omega T_{A1} C_{A1}} \right) - \frac{j T_{A2}}{\omega T_{A1} C_{A1}} \quad (1a)$$

$$b_2 = \frac{-1}{\omega T_{B2} C_{B2}} \left(T_{B1} + \frac{Y_S}{\omega T_{B1} C_{B1}} \right) - \frac{j T_{B2}}{\omega T_{B1} C_{B1}} \quad (1b)$$

$$b_3 = \frac{-1}{\omega T_{C2} C_{C2}} \left(T_{C1} + \frac{Y_S}{\omega T_{C1} C_{C1}} \right) - \frac{j T_{C2}}{\omega T_{C1} C_{C1}} \quad (1c)$$

where

$$Y_S = \frac{1}{j Z_1 \tan \theta_1} \quad (2)$$

Based on (1) and (2), the mutual admittance Y_0 from port 1 to port 2 can be expressed as

$$Y_0 = -\frac{1}{b_0} - \frac{1}{b_1} - \frac{1}{b_2} - \frac{1}{b_3} \quad (3)$$

According to the architecture shown in Fig. 1, all the parameters of the equivalent circuit constructed in Fig. 3, except Z_1 and θ_1, are constant for a given patch array with fixed substrates. As a result, the mutual admittance Y_0 is entirely determined by the shorted stubs. By properly selecting the values of Z_1 and θ_1 to achieve the condition of $Y_0 = 0$, the original coupling between the two patches can be canceled, leading to a theoretically perfect decoupling between ports 1 and 2. The above discussion presents the decoupling principle of the proposed wavetraps through an equivalent circuit. Next, a network study is proposed for determining the parameters Z_1 and θ_1.

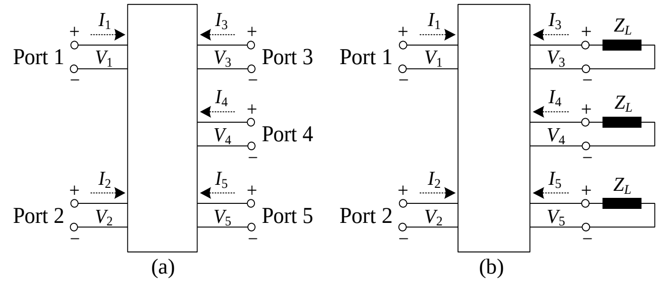

Fig. 4. (a) Five-port network of case B. (b) Two-port network of case B.

Here, three additional ports (defined as ports 3, 4, and 5) are introduced for further study, as marked in Fig. 3(a). The terminal planes of the three ports are set at the ends of the probes correspondingly. Subsequently, a five-port network of the five-port array plotted in Fig. 3(a) is constructed for the sake of analysis, as illustrated in Fig. 4(a). On the n^{th} port, the equivalent voltage and current are marked as V_n and I_n, respectively. The impedance matrix Z of the five-port network then relates the mentioned voltages and currents, expressed as

$$\begin{bmatrix} V_1 \\ V_2 \\ V_3 \\ V_4 \\ V_5 \end{bmatrix} = \begin{bmatrix} Z_{11} & Z_{12} & Z_{13} & Z_{14} & Z_{15} \\ Z_{21} & Z_{22} & Z_{23} & Z_{24} & Z_{25} \\ Z_{31} & Z_{32} & Z_{33} & Z_{34} & Z_{35} \\ Z_{41} & Z_{42} & Z_{43} & Z_{44} & Z_{45} \\ Z_{51} & Z_{52} & Z_{53} & Z_{54} & Z_{55} \end{bmatrix} \begin{bmatrix} I_1 \\ I_2 \\ I_3 \\ I_4 \\ I_5 \end{bmatrix} \quad (4)$$

Seeing that ports 3, 4, and 5 will be terminated by the shorted stubs as illustrated in Fig. 1, the five-port network can be further simplified to a two-port network as plotted in Fig. 4(b), where

$$Z_L = j Z_1 \tan \theta_1 \quad (5)$$

According to the two-port network and (4), we have

$$\begin{cases} V_3 = -Z_L I_3 = Z_{31} I_1 + Z_{32} I_2 + Z_{33} I_3 + Z_{34} I_4 + Z_{35} I_5 \\ V_4 = -Z_L I_4 = Z_{41} I_1 + Z_{42} I_2 + Z_{43} I_3 + Z_{44} I_4 + Z_{45} I_5 \\ V_5 = -Z_L I_5 = Z_{51} I_1 + Z_{52} I_2 + Z_{53} I_3 + Z_{54} I_4 + Z_{55} I_5 \end{cases} \quad (6)$$

Substituting (4) into (6), the numerical expressions of currents I_3, I_4, and I_5 can be obtained based on currents I_1 and I_2, briefly given as

$$\begin{cases} I_3 = h_3(I_1, I_2) \\ I_4 = h_4(I_1, I_2) \\ I_5 = h_5(I_1, I_2) \end{cases} \quad (7)$$

where h_3, h_4, and h_5 are the functions with the variables of I_1 and I_2. On the other hand, the impedance matrix Z' of the two-port network relates the voltages V_1 and V_2, and currents I_1 and I_2, expressed as

$$\begin{bmatrix} V_1 \\ V_2 \end{bmatrix} = \begin{bmatrix} Z'_{11} & Z'_{12} \\ Z'_{21} & Z'_{22} \end{bmatrix} \begin{bmatrix} I_1 \\ I_2 \end{bmatrix} \tag{8}$$

Then, we have

$$V_1 = Z'_{11} I_1 + Z'_{12} I_2 \tag{9}$$

Besides, we see from (4) that V_1 can be found as

$$V_1 = Z_{11} I_1 + Z_{12} I_2 + Z_{13} I_3 + Z_{14} I_4 + Z_{15} I_5 \tag{10}$$

Substituting (7) and (10) into (9), Z'_{12} can be determined as

$$Z'_{12} = Z'_{21} = -\left(Z_{12} + Z_{13} P_3 + Z_{14} P_4 + Z_{15} P_5\right)/Q \tag{11}$$

where

$$\begin{aligned} P_3 &= Z_{34}\left(Z_{45}Z_{52} - Z_{42}Z_{55}\right) + Z_{35}\left(Z_{42}Z_{54} - Z_{44}Z_{52}\right) \\ &\quad + \left[Z_{32}\left(Z_{44}+Z_{55}\right) - Z_{34}Z_{42} - Z_{35}Z_{52}\right] jZ_1 \tan\theta_1 \\ &\quad + Z_{32}\left(-Z_1^2 \tan^2\theta_1 + Z_{44}Z_{55} - Z_{45}^2\right) \end{aligned} \tag{12a}$$

$$\begin{aligned} P_4 &= Z_{43}\left(Z_{35}Z_{52} - Z_{32}Z_{55}\right) + Z_{45}\left(Z_{32}Z_{53} - Z_{33}Z_{52}\right) \\ &\quad + \left[Z_{42}\left(Z_{33}+Z_{55}\right) - Z_{32}Z_{43} - Z_{45}Z_{52}\right] jZ_1 \tan\theta_1 \\ &\quad + Z_{42}\left(-Z_1^2 \tan^2\theta_1 + Z_{33}Z_{55} - Z_{35}^2\right) \end{aligned} \tag{12b}$$

$$\begin{aligned} P_5 &= Z_{53}\left(Z_{34}Z_{42} - Z_{32}Z_{44}\right) + Z_{54}\left(Z_{32}Z_{43} - Z_{33}Z_{42}\right) \\ &\quad + \left[Z_{52}\left(Z_{33}+Z_{44}\right) - Z_{32}Z_{53} - Z_{42}Z_{45}\right] jZ_1 \tan\theta_1 \\ &\quad + Z_{52}\left(-Z_1^2 \tan^2\theta_1 + Z_{33}Z_{44} - Z_{34}^2\right) \end{aligned} \tag{12c}$$

$$\begin{aligned} Q &= \left(jZ_1\tan\theta_1 + Z_{33}\right)\left(jZ_1\tan\theta_1 + Z_{44}\right)\left(jZ_1\tan\theta_1 + Z_{55}\right) \\ &\quad - \left(jZ_1\tan\theta_1 + Z_{33}\right)Z_{45}^2 - \left(jZ_1\tan\theta_1 + Z_{44}\right)Z_{53}^2 \\ &\quad - \left(jZ_1\tan\theta_1 + Z_{55}\right)Z_{43}^2 \end{aligned} \tag{12d}$$

Based on the microwave network theory, the transmission coefficient between ports 1 and 2 can be derived [22]

$$S_{21} = S_{12} = \frac{2Z'_{21}\sqrt{R_{01}R_{02}}}{\left(Z'_{11}+Z_{01}\right)\left(Z'_{22}+Z_{02}\right) - Z'_{12}Z'_{21}} \tag{13}$$

where Z_{01} and Z_{02} are the equivalent source loads at port 1 and port 2, respectively; R_{01} and R_{02} are the real parts of Z_{01} and Z_{02}, correspondingly. It is clearly seen that there would be a transmission zero between port 1 and port 2 on the basis of

$$Z'_{12} = Z'_{21} = 0 \tag{14}$$

It is found from (11) that for the given array with fixed positions of the wavetraps, the impedance matrix Z of the five-port network is constant. By selecting a group of the parameters Z_1 and θ_1 to satisfy (14), the leakage between ports1 and 2 in case B can be well suppressed, leading to an improved isolation response at the desired frequency. Similarly, following the aforementioned discussions, the values of Z_2, Z_3, θ_2, and θ_3 can be determined, which are not detailed for brevity. Finally, for case A, after allocating the decoupling frequencies of the three groups of the wavetraps to three different but close values f_1, f_2, and f_3 correspondingly, decoupling bandwidth would be enhanced.

Case A represents the decoupling between two horizontal positioned antenna elements. For the vertical positioned 2×1 antenna array (marked as case E) shown in Fig. 5(a), it can be easily verified that the decoupling method is still effective, making the wavetraps valuable and effective for large-scale arrays. Referring to the graphical studies of Fig. 2, case E is simplified into three different cases corresponding to the three groups of the wavetraps, as illustrated in Figs. 5(b), 5(c), and 5(d). It is found that the configurations of case B and case F are mirror symmetrical. This denotes that ports 3 and 4 in case F would be decoupled on condition that ports 1 and 2 are decoupled in case B. Same symmetry is observed between cases C and G, cases D and H. In view of the symmetry, it can be concluded that the 45º-polarized configuration features a simpler mutual coupling response compared to those configurations with other polarized directions. For example, the couplings through the horizontal pair shown in Fig. 2(a) and the vertical pair plotted in Fig. 5(a) would be generally different if the antenna elements are vertical or horizontal polarized. This implies that more wavetraps are required, leading to a more complicated decoupling approach. According to the discussions, the 45º-polarized configuration is more attractive in this case for large-scale array applications. Therefore, we select the 45º-polarized patch antenna as the study case and utilize the proposed wavetraps to achieve the decoupling purpose.

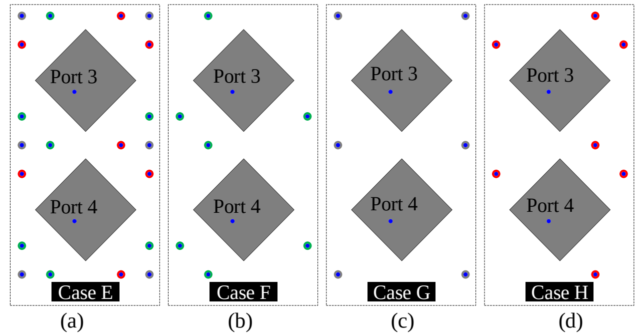

Fig.5. Configurations of the 2×1 antenna array integrated with the proposed decoupling technique. (a) Case E. (b) Case F. (c) Case G. (d) Case H.

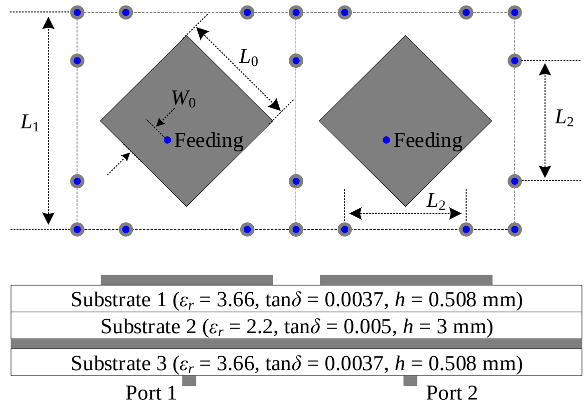

Fig. 6. Physical dimensions of a two-element patch array integrated with the proposed decoupling wavetraps, where L_0 = 17.0, L_1 = 30.6, L_2 = 17.0, W_0 = 4.7 (Units: mm). The diameters of the pad and the probe are 2.0 mm and 1.0 mm, respectively.

III. NUMERICAL STUDY OF THE 1×2 ARRAY

In this section, a series of numerical studies are carried out to give further investigations on the decoupling performance of a 1×2 patch array. Fig. 6 depicts the configuration of the array. Please note that the stacked substrates, i.e., substrate 1 and substrate 2, are utilized to obtain a wideband patch antenna,

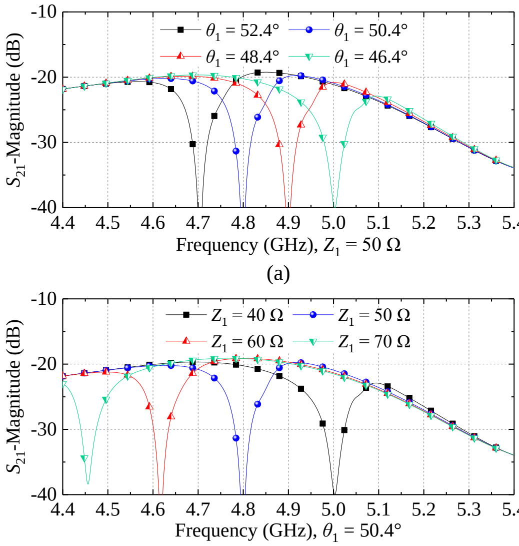

Fig. 7. Calculated transmission responses between ports 1 and 2 in case B with different (a) θ_1 and (b) Z_1.

which has no specified contribution to the proposed decoupling method. As for substrate 3, it is served as the support of the feeding lines and the shorted stubs, whose dielectric constant is properly selected to make sure that all the microstrip lines can be fabricated with compact sizes. Prior to operating the analysis, full-wave simulator Computer Simulation Technology (CST) is used to get the required impedance matrices. Here, the 22-port model shown in Fig. 2(a) is utilized for the full-wave simulations, and the desired impedance matrices are derived on condition that other non-related ports are terminated with matched loads. For example, to get the impedance matrix of case B, the other 17 ports in case A are terminated, and the five-port network is constructed. Once the desired impedance matrices are obtained, the transmission responses between port 1 and port 2 in cases B, C, and D can be calculated accordingly, based on (13) for the given values of Z_i and θ_i. Here, all electrical lengths are referred at the center frequency, which is 4.9 GHz in this study.

Fig. 7 illustrates the calculated transmission responses between ports 1 and 2 in case B versus different Z_1 and θ_1. It is observed from Fig. 7(a) that for the given characteristic impedance of Z_1 = 50 Ω, a transmission zero can be realized at certain frequencies with specified θ_1. The calculated isolation is improved from around 18 dB to higher than 30 dB at the desired frequency, compared to the one without decoupling. Similar results can be observed for cases C and D, and some calculated responses are depicted in Fig. 8, which are not detailed for brevity. It is revealed from Fig. 8(a) that the decoupling levels contributed from case C are not as high as those from cases B and D. The probable reason is that the distances between the wavetraps belonging to group D2 and the radiation patch are larger than those in other cases, leading to a lower decoupling level. The graphical studies provided in Figs. 7 and 8 describe the decoupling performance of the proposed wavetraps separately, corresponding to the separated cases B, C and D. Next, the coupling response of case A where all wavetraps are integrated is further studied.

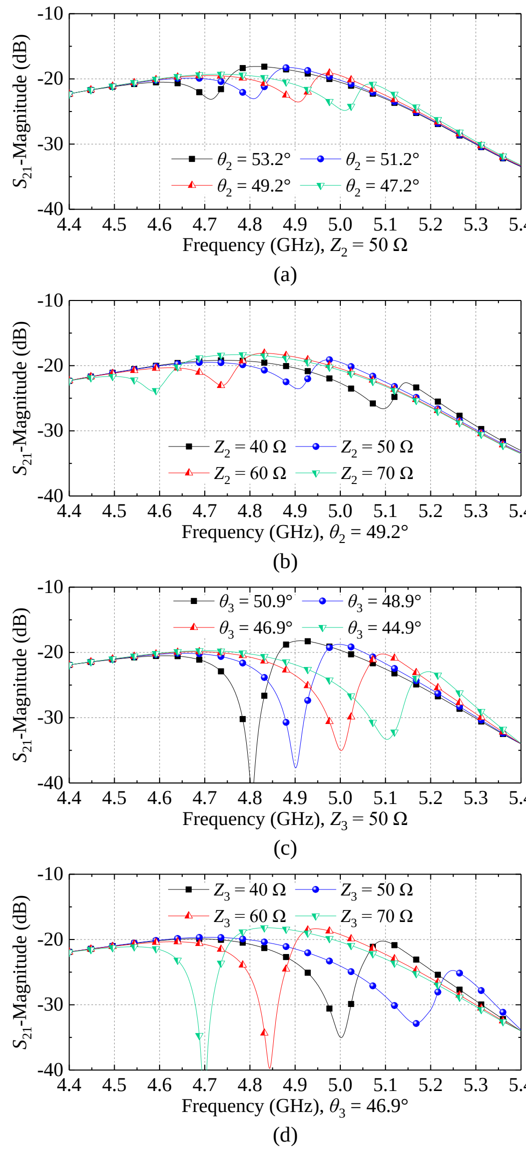

Fig. 8. Calculated transmission responses between ports 1 and 2 with different (a) θ_2 and (b) Z_2 in case C, with different (c) θ_3 and (d) Z_3 in case D.

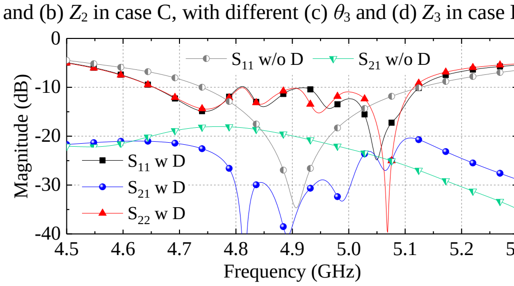

Fig. 9. Calculated transmission responses of case A with the decoupling wavetraps, where $Z_1 = Z_2 = Z_3$ = 50.0 Ω, θ_1 = 50.4°, θ_2 = 49.2°, θ_3 = 46.9°.

For case A, the three transmission zeros contributed from the three groups of wavetraps are allocated at three frequencies as f_1 = 4.8 GHz, f_2 = 4.9 GHz, and f_3 = 5.0 GHz. The parameters of the transmission lines are determined based on the graphical studies plotted in Fig. 7 and Fig. 8. Illustrated in Fig. 9 are the calculated transmission responses of the 1×2 array with all three groups of the decoupling wavetraps. The full-wave simulated S_{11} and S_{21} without decoupling are also depicted in

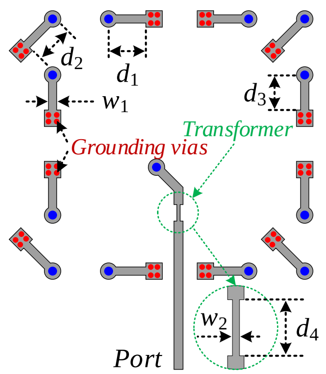

(a)

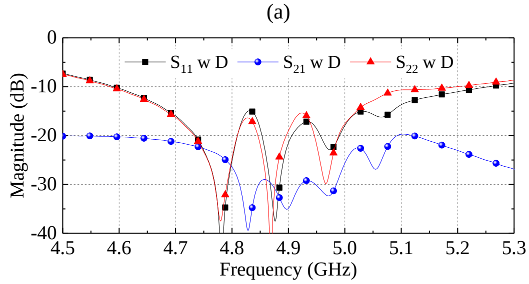

(b)

Fig. 10. (a) Physical sizes of the network layer, including the feeding line and the wavetraps, where d_1 = 4.5, d_2 = 4.45, d_3 = 4.25, d_4 = 2.0, w_1 = 1.0, w_2 = 0.4 (Units: mm). (b) Full-wave simulated S-parameters of the 1×2 antenna array with the proposed decoupling method and the transformer for impedance matching.

Fig. 9. It is seen that three transmission zeros of S_{21} are observed at the desired frequencies after decoupling, resulting in the significantly enhanced isolation performance, from 18 dB to better than 28.5 dB within the band of 4.8-5.0 GHz. Fig. 9 also verifies that the decoupling performance of the three groups of the wavetraps are independent, making the design and the realization to be very simple and effective. Since the return-loss levels are influenced on both two ports, a simple impedance transformer is employed for each port to improve the impedance matching, which will be mentioned later.

Fig. 10(a) describes the physical dimensions of the feeding network layer including decoupling wavetraps. The transmission-line-based transformer marked in the green dash block is utilized for impedance matching. Fig. 10(b) depicts the full-wave simulated results of the 1×2 array based on the layout shown in Fig. 10(a). It is observed that the isolation performance is consistent with the calculated one plotted in Fig. 9. Seeing that an additional but simple transformer is employed at each antenna port, the impedance responses are enhanced compared to those without the transformer. Furthermore, a comparison of surface current distributions between the arrays without and with the proposed wavetraps is given in Fig. 11. It is found that before decoupling, obvious currents are induced on the right patch when the left patch is excited, denoting a strong mutual coupling. After employing the wavetraps, the induced current has been significantly suppressed. Besides, the result implies that only a very small amount of 135°-directed electric field is excited on the right patch, resulting in a high isolation level between the two ports since the patches are 45° polarized.

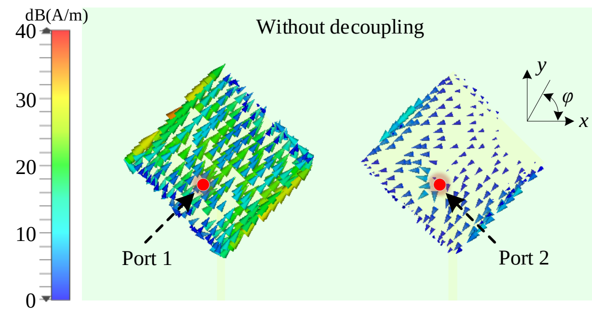

(a)

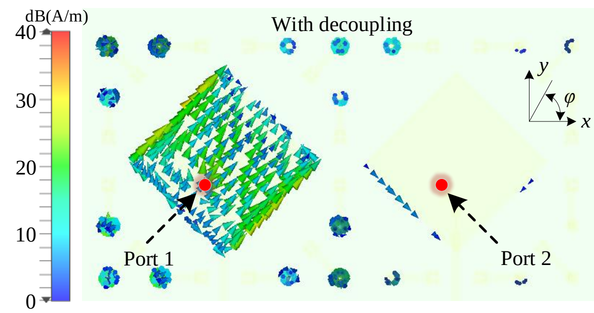

(b)

Fig. 11. Full-wave simulated surface current distributions of the patches in the 1×2 antenna arrays at 4.9 GHz. (a) Without decoupling. (b) With decoupling.

To clarify the realization of the proposed decoupling wavetrap structures for the 1×2 antenna array more clearly, a design procedure involving four steps is summarized, given as

Step 1) Separating the wavetraps into three groups D1, D2, and D3 as plotted in Fig. 2, and obtaining the required impedance matrices through full-wave simulations;

Step 2) Constructing the corresponding network models as shown in Fig. 4, and selecting the three frequencies f_1, f_2, and f_3, where transmission zeros would be generated; determining the numerical values of the parameters Z_1, Z_2, Z_3, θ_1, θ_2, and θ_3 by following the derivations of (4)-(14);

Step 3) Integrating all numerically-determined wavetraps together into case A, and determining the transformer for further impedance matching by investigating the input impedance response at the interfaces of antenna ports;

Step 4) Transforming all numerical parameters into physical sizes, and determining the final layout of the proposed decoupling wavetraps by using full-wave simulations for finely tuning.

Next, two 45°-polarized antenna arrays integrated with the proposed decoupling wavetraps are developed and measured. The full-wave simulated and measured results will be provided in Section IV.

IV. Measurements of Two Demonstrators

To demonstrate the performance of the proposed decoupling method for practical array applications, two examples are conducted in this section. The first case is a 1×8 45°-polarized antenna array, and the second one is a 4×2 45°-polarized antenna array. The configurations plotted in Figs. 6 and 10 are utilized as the practical array element and the wavetraps, and identical physical dimensions are employed for both cases.

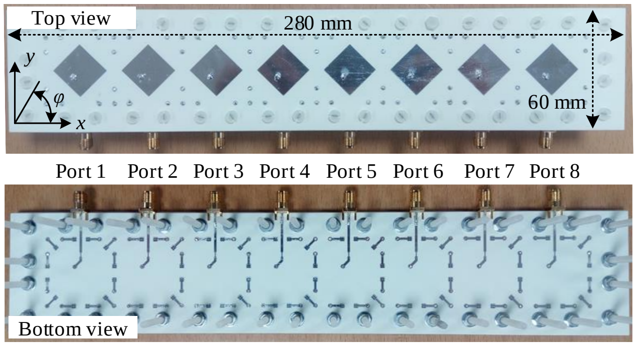

Fig. 12. Photos of the decoupled 1×8 antenna array.

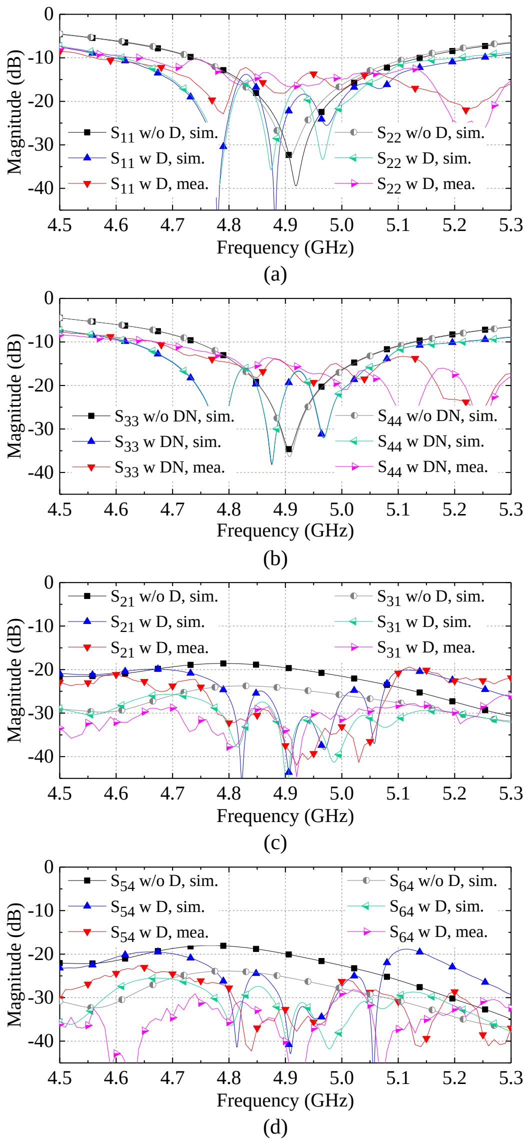

Fig. 13. Measured and simulated S-parameters of the representative ports in the 1×8 array. (a) S_{11} and S_{22}. (b) S_{33} and S_{44}. (c) S_{21} and S_{31}. (d) S_{54} and S_{64}.

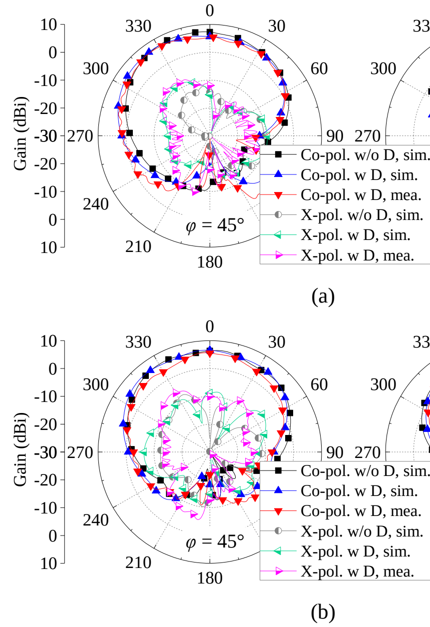

Fig. 14. Measured and simulated radiation performance of the representative ports in the 1×8 antenna array. (a) Port 1. (b) Port 4.

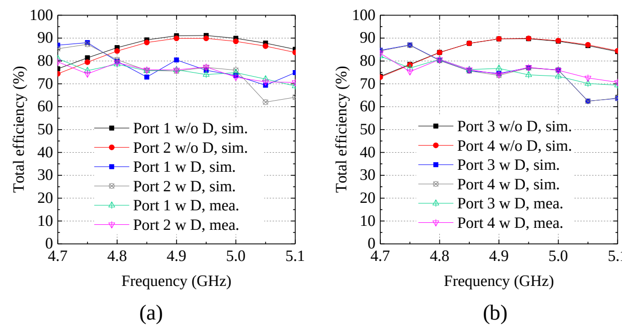

Fig. 15. Measured and simulated total efficiency of the representative ports in the 1×8 antenna array. (a) Ports 1 and 2. (b) Ports 3 and 4.

A. 1×8 antenna array

Fig. 12 shows the photos of the developed 1×8 antenna array with the proposed decoupling wavetraps. The overall size is 280×60×4.016 mm^3. The demonstrator is fully measured. The S parameters and the radiation performance are tested by utilizing the Agilent 85309N network analyzer and the SATIMO SG24L spherical near-field scanner, respectively.

Fig. 13 depicts the measured and simulated S parameters of some representative ports, with and without using the decoupling wavetraps. It is seen that the impedance bandwidths are slightly expanded after decoupling for both simulated and measured results. For the frequency band from 4.8 to 5.0 GHz, the coupling levels between two adjacent antenna elements, e.g., S_{21} and S_{54}, are reduced from –18.0 dB to lower than –26.0 dB. Moreover, the couplings between non-adjacent elements, e.g., S_{31} and S_{64}, are also suppressed to less than –28.0 dB. Notice that since the S parameters are measured in lab environment, there are some fluctuations for the measurements due to the reflections as well as some uncertain influence in practice such as fabrication/assembling errors.

The far-field radiation patterns of ports 1 and 4 are illustrated in Fig. 14. Good consistency between the simulated and measured results for both with and without the proposed decoupling wavetraps is observed. This is the same for other unmentioned ports, which are not given for brevity. The total efficiencies are also provided, as shown in Fig. 15. It is found that within the frequency band of 4.8 to 5.0 GHz, the proposed decoupling wavetraps lead to some deteriorations on the total efficiencies, from 89%-90% to 75%-80% due to the conductive loss at wavetraps. The worst degradation of the total efficiency

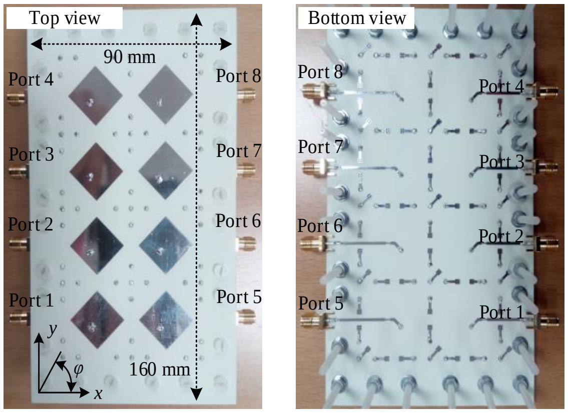

Fig. 16. Photos of the decoupled 4×2 antenna array.

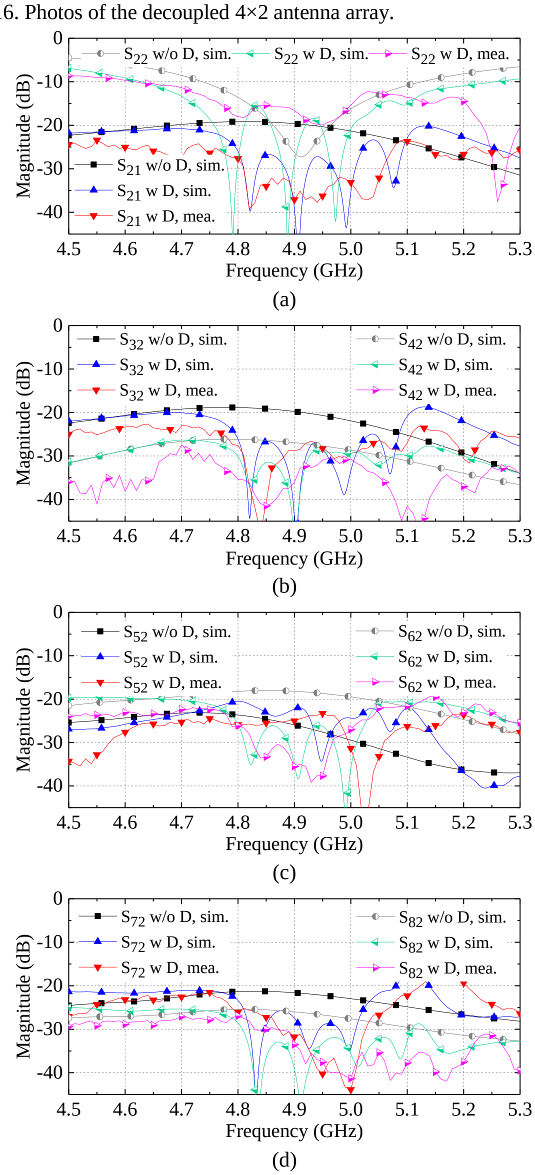

Fig. 17. Measured and simulated S-parameters of the representative ports in the 4×2 array. (a) S_{21} and S_{22}. (b) S_{32} and S_{42}. (c) S_{52} and S_{62}. (d) S_{72} and S_{82}.

is approximately 15%, indicating an insertion loss of 0.7 dB. Based on the above discussions, the developed 1×8 antenna array features well-designed decoupling performance, where both adjacent and non-adjacent elements are decoupled.

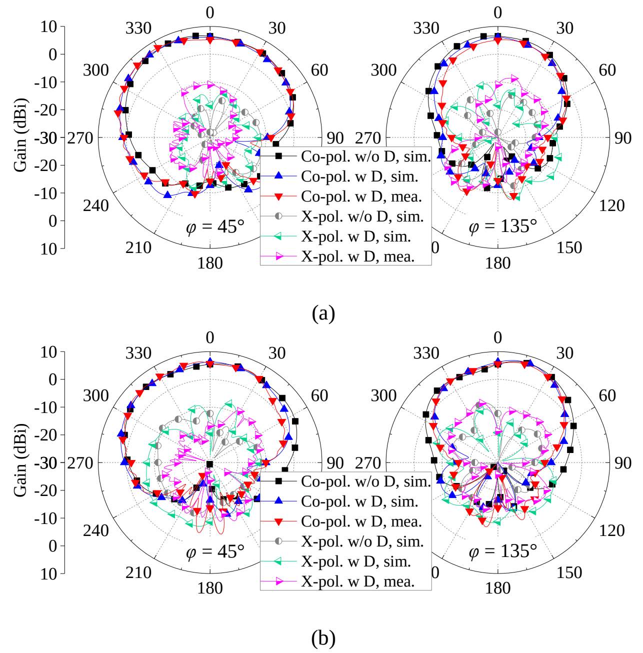

Fig. 18. Measured and simulated radiation performance of the representative ports in the 4×2 antenna array. (a) Port 1. (b) Port 2.

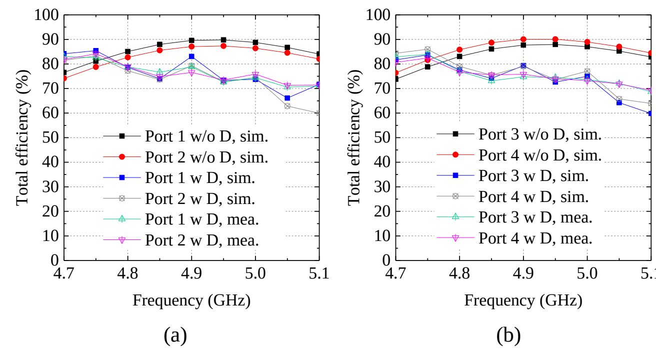

Fig. 19. Measured and simulated total efficiency of the representative ports in the 2×4 antenna array. (a) Ports 1 and 2. (b) Ports 3 and 4.

B. 4×2 antenna array

As shown in Fig. 16, a 4×2 antenna array with the proposed decoupling wavetraps is also developed and assembled. Same with the 1×8 array, the 4×2 antenna array is fully tested. Here, the results related to port 2 is chosen as the representative port for analysis. Fig. 17 provides the impedance and isolation responses of the developed demonstrator. The impedance performance is similar to those of the 1×8 antenna array, featuring wideband responses. The couplings between adjacent elements, e.g., S_{32} and S_{62}, are reduced from –18.0 dB to lower than –25.0 dB among the bandwidth of 4.8-5.0 GHz. The leakages between the non-adjacent elements are also degraded. Moreover, the isolation between diagonal pairs are not influenced or even improved, although the decoupling between these pairs of elements are not considered during the analysis. For instance, S_{52} is still kept at a low level of less than –23.5 dB, and S_{72} is reduced to less than –30.0 dB from 4.82 to 5.3 GHz.

The measured radiation patterns and total efficiencies of the 4×2 antenna array are illustrated in Fig. 18 and Fig. 19, respectively. For the radiation patterns, good consistency between the simulated and measured results for both with and

TABLE I
PERFORMANCE COMPARISONS AMONG SOME RECENTLY PUBLISHED AND THE PROPOSED DECOUPLING TECHNIQUES

Ref./Year	[6]/2017	[17]/2015	[20]/2019	[21]/2019	**This work**
Decoupling method	Decoupling surface	Transmission line	Near-field resonator	Transmission line	Wavetrap structure
Antenna type	Microstrip patch	Microstrip patch	Microstrip patch	Microstrip patch	Microstrip patch
Array configuration & center frequency	1×8: 2.45 GHz 2×2: 3.5 GHz	1×16: 7.7 GHz	1×8: 2.37 GHz 1×2: 2.45 GHz	2×2: 2.45 GHz 4×4: 4.9 GHz [a]	1×8: 4.9 GHz 4×2: 4.9 GHz
Center distance among adjacent elements	1×8: 0.45λ_0 2×2: 0.52λ_0-0.7λ_0	0.5λ_0	1×8: 0.47λ_0 1×2: 0.58λ_0	2×2: 0.5λ_0 4×4: 0.5λ_0	1×8: 0.5λ_0 4×2: 0.5λ_0
Profile(Thickness)	1×8: 0.29λ_0 2×2: 0.29λ_0	0.22λ_0	1×8: 0.05λ_0 1×2: 0.07λ_0	2×2: 0.045λ_0 4×4: 0.12λ_0	1×8: 0.07λ_0 4×2: 0.07λ_0
Impedance bandwidth ($S_{11} \leq -10$ dB)	1×8: 2.4-2.52 GHz 2×2: 3.2-4.0 GHz	7.1-7.9 GHz	1×8: 2.243-2.252 GHz 1×2: 2.38-2.53 GHz	2×2: 2.387-2.527 GHz 4×4: 4.8-5.0 GHz	1×8: 4.65-5.3 GHz 4×2: 4.65-5.3 GHz
Isolation between adjacent elements	1×8: ≥ 22.5 dB (2.4-2.5 GHz)	≥ 25.0 dB (7.1-7.8 GHz)	1×8: ≥ 20.0 dB (2.237-2.246 GHz)	2×2: ≥ 25.0 dB (2.435-2.47 GHz)	1×8: ≥ 26.0 dB (4.8-5.0 GHz)
	2×2: ≥ 25.0 dB (3.3-3.8 GHz)		1×2: ≥ 20.0 dB (2.38-2.53 GHz)	4×4: ≥ 25.0 dB (4.884-4.923 GHz)	4×2: ≥ 26.5 dB (4.8-5.0 GHz)
Decoupling between non-adjacent elements	No	No	No	No	Yes
Isolation between non-adjacent elements	1×8: ≥ 24.0 dB	≥ 25.0 dB	Not given	4×4: ≥ 24.3 dB	1×8: ≥ 28.0 dB 4×2: ≥ 23.5 dB
Total efficiency among decoupled bandwidth	Not given	Not given	Not given	2×2: 84%-90% 4×4: 70%-82%	1×8: 75%-80% 4×2: 73%-80%
Insertion loss caused by decoupling	Not given	Not given	Not given	≤ 0.45 dB	≤ 0.7 dB

[a] The results of the 4×4 array proposed in [21] are all simulated results.

without the decoupling wavetraps are obtained. Similar to the 1×8 array, some deteriorations on the total efficiency are found here. The measured total efficiency of port 4 is with the worst degradation of 14% within the band from 4.8 to 5.0 GHz, corresponding to an insertion loss of around 0.65 dB.

For performance comparison, Table I summarized some recently published decoupling methods as well as the proposed wavetrap-based technique. Different from the published methods with bulky system [6], complicated decoupling network [17], narrow band [21] or significant influence on operation frequency [20], the proposed scheme is simple with low insertion loss, and features simplicity in implementation and applicability to large-scale arrays including massive MIMO and phased arrays for communications and radar applications.

V. CONCLUSION

To suppress the strong mutual coupling between both adjacent and non-adjacent elements within antenna arrays, a wavetrap-based decoupling technique is proposed in this work. The presented wavetrap structure is compact, simple, and can be readily realized, making it valuable for large-scale antenna arrays such as massive MIMO antennas and phased arrays. Furthermore, two design examples centered at 4.9 GHz are provided and tested. The full-wave simulated and measured results denote that the proposed scheme features low profile with loss insertion loss and nearly no effect on radiation patterns.

REFERENCES

[1] À. O. Martínez, J. Ø. Nielsen, E. D. Carvalho, and P. Popovski, “An experimental study of massive MIMO properties in 5G scenarios,” *IEEE Trans. Antennas Propag.*, vol. 66, no. 12, pp. 7206-7215, Dec. 2018.

[2] E. G. Larsson, O. Edfors, F. Tufvesson, and T. L. Marzetta, “Massive MIMO for next generation wireless systems,” *IEEE Commun. Mag.*, vol. 52, no. 2 pp. 186-195, Feb. 2014.

[3] W. L. Stutzman and G. A. Thiele, “Array antennas,” in *Antenna Theory and Design*, 3th ed., John Wiley & Sons, 2012, ch. 8, pp. 315–320.

[4] X. Chen, S. Zhang, and Q. Li, “A review of mutual coupling in MIMO systems.” *IEEE Access*, vol. 6, pp. 24706-24719, 2018.

[5] L. Savy and M. Lesturgie, “Coupling effects in MIMO phased array,” in *Proc. IEEE Radar Conf.*, Philadelphia, PA, USA, May 2016, pp. 1–6.

[6] K.-L. Wu, C. Wei, X. Mei, and Z.-Y. Zhang, “Array-antenna decoupling surface,” *IEEE Trans. Antennas Propag.*, vol. 65, no. 12, pp. 6728-6738, Dec. 2017.

[7] C. Fager, X. Bland, K. Hausmair, et al. “Prediction of smart antenna transmitter characteristics using a new behavioral modeling approach,” *IEEE MTT-S Int. Microw. Symp.*, Tampa, US, Jun. 1-6, 2014, pp. 1-4.

[8] B. Wang, Y. Chang, and Y. Sun, “Performance of the large-scale adaptive array antennas in the presence of mutual coupling,” *IEEE Trans. Antennas Propag.*, vol. 64, no. 6, pp. 2236-2245, Jun. 2016.

[9] K.-H. Chen and J.-F. Kiang, “Effect of mutual coupling on the channel capacity of MIMO systems,” *IEEE Trans. Veh. Technol.*, vol. 65, no. 1, pp. 398–403, Jan. 2016.

[10] J.-Y. Lee, S.-H. Kim, and J.-H. Jang, “Reduction of mutual coupling in planar multiple antenna by using 1-D EBG and SRR structures,” *IEEE Trans. Antennas Propag.*, vol. 63, no. 9, pp. 4194-4198, Sep. 2015.

[11] E. Rajo-Iglesias, Ó. Quevedo-Teruel, and L. Inclan-Sanchez, “Mutual coupling reduction in patch antenna arrays by using a planar EBG structure and a multilayer dielectric substrate,” *IEEE Trans. Antennas Propag.*, vol. 56, no. 6, pp. 1648-1655, Jun. 2008.

[12] Z. Qamar, U. Naeem, S. A. Khan, M. Chongcheawchamnan, and M. F. Shafique, “Mutual coupling reduction for high-performance densely packed patch antenna arrays on finite substrate,” *IEEE Trans. Antennas*

Propag., vol. 64, no. 5, pp. 1653-1660, May 2016.

[13] C.-H. Wu, C.-L. Chiu, and T.-G. Ma, “Very compact fully lumped decoupling network for a coupled two-element array,” *IEEE Antennas Wireless Propag. Lett.*, vol. 15, pp. 158-161, 2016.

[14] S. N. Venkatasubramanian, L. Li, A. Lehtovuori, C. Icheln, and K. Haneda, “Impact of using resistive elements for wideband isolation improvement,” *IEEE Trans. Antennas Propag.*, vol. 65, no. 1, pp. 52-62, Jan. 2017.

[15] H. Meng and K.-L. Wu, “An LC decoupling network for two antennas working at low frequencies,” *IEEE Trans. Microw. Theory Tech.*, vol. 65, no. 7, pp. 2321-2329, Jul. 2017.

[16] Y.-F. Cheng and K.-K. M. Cheng, “A novel dual-band decoupling and matching technique for asymmetric antenna arrays,” *IEEE Trans. Microw. Theory Tech.*, vol. 6, no. 5, pp. 2080-2089, May. 2018.

[17] R.-L. Xia, S.-W. Qu, P.-Fa Li, D.-Q. Yang, S. Yang, and Z.-P. Nie, “Wide-angle scanning phased array using an efficient decoupling network,” *IEEE Trans. Antennas Propag.*, vol. 63, no. 11, pp. 5161-5165, Nov. 2015.

[18] J. Sui and K.-L. Wu, “Self-curing decoupling technique for two inverted-F antennas with capacitive loads,” *IEEE Trans. Antennas Propag.*, vol. 66, no. 3, pp. 1093-1101, Mar. 2018.

[19] Y. M. Pan, X. Qin, Y. X. Sun and S. Y. Zheng, “A simple decoupling method for 5G millimeter wave MIMO dielectric resonator antennas,” *IEEE Trans. Antennas Propag.*, vol. 67, no. 4, pp. 2224-2234, Apr. 2019.

[20] M. Li, B. G. Zhong, and S. W. Cheung, “Isolation enhancement for MIMO patch antennas using near-filed resonators as coupling-mode transducers,” *IEEE Trans. Antennas Propag.*, vol. 67, no. 2, pp. 755-764, Feb. 2019.

[21] Y.-M. Zhang, S. Zhang, J.-L. Li, and G. F. Pedersen, “A transmission-line-based decoupling method for MIMO antenna arrays,” *IEEE Trans. Antennas Propag.*, vol. 67, no. 5, pp. 3117-3131, May 2019.

[22] D. A. Frickey, “Conversions between S, Z, Y, H, ABCD, and T parameters which are valid for complex source and load impedances,” *IEEE Trans. Microw. Theory Tech.*, vol. 42, no. 2, pp. 205-211, Feb. 1994.

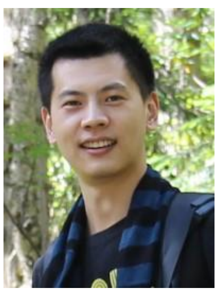

Yi-Ming Zhang (S’17-M’19) received the B.S. degree from Central China Normal University in 2008, the M.S. and Ph.D. degrees from University of Electronic Science and Technology of China in 2014 and 2019, respectively. From 2018 to 2019, he was a guest researcher with the Antenna, Propagation and Millimeter-wave Systems (APMS) Section, Aalborg University, Denmark, where he currently works as a Post Doctor. His current research interests include massive MIMO antenna decoupling, single-channel full-duplex antennas, and passive RF and microwave components.

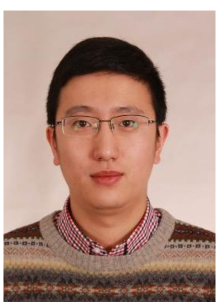

Shuai Zhang (SM’18) received the B.E. degree from the University of Electronic Science and Technology of China, Chengdu, China, in 2007 and the Ph.D. degree in electromagnetic engineering from the Royal Institute of Technology (KTH), Stockholm, Sweden, in 2013. After his Ph.D. studies, he was a Research Fellow at KTH. In April 2014, he joined Aalborg University, Denmark, where he currently works as Associate Professor. In 2010 and 2011, he was a Visiting Researcher at Lund University, Sweden and at Sony Mobile Communications AB, Sweden, respectively. He was also an external antenna specialist at Bang & Olufsen, Denmark from 2016-2017. He has coauthored over 50 articles in well-reputed international journals and over 15 (US or WO) patents. His current research interests include: mobile terminal mmwave antennas, biological effects, CubeSat antennas, Massive MIMO antenna arrays, UWB wind turbine blade deflection sensing, and RFID antennas.

Jia-Lin Li received the M. S. degree from the University of Electronic Science and Technology of China (UESTC), Chengdu, China, in 2004, and the Ph. D. degree from the City University of Hong Kong, Hong Kong, in 2009, both in electronic engineering.

From September 2005 to August 2006, he was a Research Associate with the Wireless Communication Research Center, City University of Hong Kong, Hong Kong. Since September 2009, he has been with the School of Physical Electronics, UESTC, where he is currently a Professor. His research interests include microwave/millimeter-wave antenna and arrays, circuits and systems, interactions between microwave and complex medium, and so on.

Gert Frølund Pedersen was born in 1965. He received the B.Sc. and E.E. (Hons.) degrees in electrical engineering from the College of Technology in Dublin, Dublin Institute of Technology, Dublin, Ireland, in 1991, and the M.Sc.E.E. and Ph.D. degrees from Aalborg University, Aalborg, Denmark, in 1993 and 2003, respectively. Since 1993, he has been with Aalborg University where he is a Full Professor heading the Antennas, Propagation and Millimeter-wave Systems LAB with 25 researchers. He is also the Head of the Doctoral School on wireless communication with some 40 Ph.D. students enrolled. His research interests include radio communication for mobile terminals especially small antennas, diversity systems, propagation, and biological effects. He has published more than 500 peer reviewed papers, 6 books, 12 book chapters and holds over 50 patents. He has also worked as a Consultant for developments of more than 100 antennas for mobile terminals including the first internal antenna for mobile phones in 1994 with lowest SAR, first internal triple-band antenna in 1998 with low SAR and high TRP and TIS, and lately various multiantenna systems rated as the most efficient on the market. He has worked most of the time with joint university and industry projects and have received more than 21 M$ in direct research funding. He is currently the Project Leader of the RANGE project with a total budget of over 8 M$ investigating high performance centimetre/millimetre-wave antennas for 5G mobile phones. He has been one of the pioneers in establishing over-the-air measurement systems. The measurement technique is now well established for mobile terminals with single antennas and he was chairing the various COST groups with liaison to 3GPP and CTIA for over-the-air test of MIMO terminals. He is currently involved in MIMO OTA measurement.